Optical trap stiffness in the presence and absence of spherical aberrations

Vermeulen, K.C.; Wuite, G.J.L.; Stienen, G.J.M.; Schmidt, C.

published in
Applied Optics
2006

DOI (link to publisher)
10.1364/AO.45.001812

document version
Publisher's PDF, also known as Version of record

Optical trap stiffness in the presence and absence of spherical aberrations

Karen C. Vermeulen, Gijs J. L. Wuite, Ger J. M. Stienen, and Christoph F. Schmidt

Optical traps are commonly constructed with high-numerical-aperture objectives. Oil-immersion objectives suffer from spherical aberrations when used for imaging in aqueous solutions. The effect of spherical aberrations on trapping strength has been modeled by approximation, and only a few experimental results are available in the case of micrometer-sized particles. We present an experimental study of the dependence of lateral and axial optical-trap stiffness on focusing depth for polystyrene and silica beads of 2 μm diameter by using oil- and water-immersion objectives. We demonstrate a strong depth dependence of trap stiffness with the oil-immersion objective, whereas no depth dependence was observed with the water-immersion objective.

OCIS codes: 00.2190, 140.0140, 140.7010, 180.0180.

1. Introduction

In 1986, Ashkin *et al.* first demonstrated laser optical trapping,[1] which can be used to apply piconewton forces to micrometer-sized refractile particles when positioned within tens of nanometers of a diffraction-limited laser focus. These force and displacement magnitudes make the technique well suited for single-molecule studies. Typically, silica or polystyrene beads of diameters between 100 nm and 10 μm are trapped and used as handles to manipulate proteins or macromolecules.[2–12] A single-beam optical trap requires a highly convergent laser beam focused into a sample chamber. This calls for an objective with a high numerical aperture (NA). Oil-immersion objectives are often preferred for this purpose.

When an oil-immersion objective is used for trapping in aqueous solutions, spherical aberration occurs (see Fig. 1) because of the refractive index mismatch between oil and coverslip ($n \approx 1.55$) and water ($n \approx 1.33$). Rays at a large angle to the optical axis, originating from the outer ring of the objective pupil, are focused closer to the coverslip surface than small-angle rays, originating from the central part of the pupil. Spherical aberration thus causes the focus to be smeared out and the maximum light intensity in the focus to decrease with increasing distance from the glass surface. As a result, the trap stiffness (κ) decreases. Since trapping involves a competition between (dissipative) scattering and (conservative) gradient components of the force,[1] widening of the focus will make the trap unstable at some distance from the surface, which will depend on the bead material. In contrast to oil-immersion objectives, water-immersion objectives do not suffer from spherical aberrations when used to focus into a watery environment (see Fig. 1). Thus it is expected that trap stiffness will not depend on the distance of the bead to the surface when a water-immersion objective is used.[13]

In most optical-trapping experiments it is important to know the exact trap stiffness to be able to quantify forces. It is therefore essential to know the full dependence of the optical-trap stiffness on the distance to the surface. The depth dependence of the trap stiffness that is due to spherical aberration is discussed in two recent theoretical papers in which different approximations are described. Rohrbach and Stelzer[14] give a detailed analysis of the trap stiffness in the presence of spherical aberrations based on the propagation of electromagnetic waves. Their treatment is valid for beads up to a diameter of approximately one wavelength. Fällman and Axner[15] give an analysis of trapping force for micrometer-sized beads by using a ray-optics approximation. This

K. C. Vermeulen, G. J. L. Wuite (gwuite@nat.vu.nl), and C. F. Schmidt are with the Department of Physics and Astronomy, and Laser Centre, Vrije Universiteit Amsterdam, De Boelelaan 1081, 1081 HV Amsterdam, The Netherlands. G. J. M. Steinem is with the Laboratory for Physiology, Institute for Cardiovascular Research, VU Medical Center, Van der Boechorststraat 7, 1081 BT Amsterdam, The Netherlands.

Received 11 April 2005; revised 31 August 2005; accepted 16 September 2005; posted 26 September 2005 (Doc. ID 61474).

0003-6935/06/081812-08$15.00/0

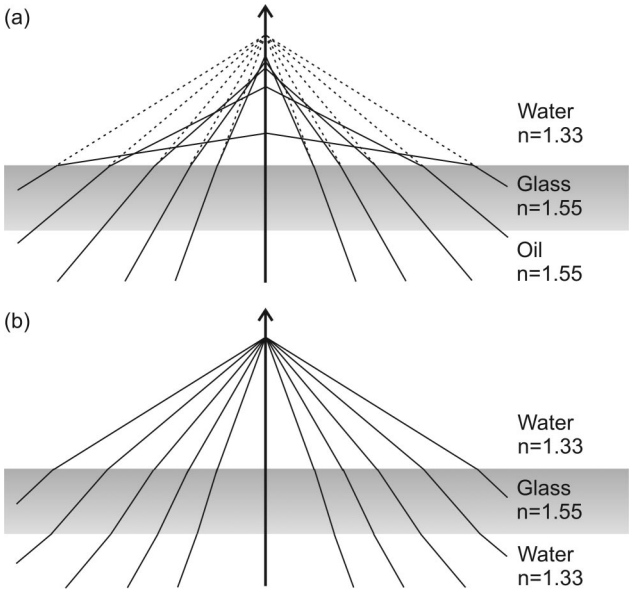

Fig. 1. (a) Ray-optics sketch of a beam focused into water with an oil-immersion objective through a glass–water interface. Spherical aberration occurring at the glass–water interface produces an elongated focus with rays at critical angle for total internal reflection remaining at the surface. Rays with a small angle to the optical axis are focused deeper in the sample than rays with a larger angle to the optical axis. Dotted lines indicate where the focal point would have been in the absence of spherical aberrations (matching refractive indices). (b) When a water-immersion objective is used, the beam is refracted at both the water–glass and the glass–water interfaces, resulting in an undistorted focus, even at large distances from the surface.

approach is appropriate for the bead size used in many single-molecule studies.[5–9,11,12] Their study, however, discusses only the axial and not the lateral trap stiffness. The latter is often more relevant in experiments. Some experimental data are available to compare with the theoretical predictions,[16–20] but these studies mostly deal with bead sizes smaller than or comparable with the wavelength of the light used for trapping.

In this paper we explore the dependence of lateral and axial trap stiffnesses for beads of ~2 μm in diameter on the distance to the surface in the presence and absence of spherical aberration for two commonly used bead materials, polystyrene and silica. We reconfirm that the trap stiffness when a water-immersion objective is used is independent of the distance to the surface. Using this feature, we explore the changes in the viscous drag coefficient near the coverslip surface that are due to boundary effects, and we use this as a method to determine the distance of the bead to the surface.

2. Materials and Methods

A. Experimental Setup and Sample Preparation

Two different setups, described in more detail elsewhere,[21–23] were used, both in a standard single-beam optical-trapping configuration. The first uses a water-immersion objective (60×, Nikon Plan Apo, NA of 1.2) with a back aperture of ~9 mm to focus a 1064 nm laser beam (Millenia IR, Nd:YVO_4, 10 W cw, Spectra-Physics, Mountain View, California) into the sample chamber. Just before entering the objective, the beam was 11.5 mm with an approximately top-hat shape and a power of 320 mW. A quadrant photodiode (UDT Sensors, Inc., Hawthorne, California), placed in a position conjugate to the back focal plane of the condenser that collects the laser light downstream from the trap, was used to detect the position (x, y) of the bead in the plane normal to the optical axis.[24]

The second setup uses an oil-immersion objective (100×, Zeiss Neofluar, NA of 1.3) with a back aperture of 4.2 mm to focus a 1064 nm laser (Nd:YAG, 4 W cw, Compass 1064-4000M, Coherent, Santa Clara, California) into the sample chamber. Just before entering the objective, the beam was a Gaussian with 3.9 mm FWHM and had a power of 200 mW. A quadrant photodiode (YAG444-4A, Perkin-Elmer, Vaudreuil, Canada), again back-focal-plane conjugate, was used to measure the lateral position of the bead in the trap. A piezo-controlled stage (Nano-LP-100, Mad City Labs, Madison, Wisconsin) was used to move the sample with respect to the trap.

We measured the axial position of the bead in both setups by monitoring the total intensity recorded by the quadrant diode. Axial fluctuations modulate by interference the total amount of light collected with a finite aperture, and, in a range of the order of 1 μm around the focus, total intensity change is proportional to axial displacement.[25]

For both setups the signals of the quadrant photodiode were processed and amplified by custom-built analog electronics, then digitized by a 200 kHz analog-to-digital converter (AD16/ChicoPlus, Innovative Integration, Simi Valley, California), processed, and saved to file with custom-designed software (LabVIEW, National Instruments, Austin, Texas). Data recorded included the x- and the y-displacement signals of the bead in the trap and the averaged total light intensity on the quadrant photodiode. In the case of the setup with the oil-immersion objective, the z position of the piezo-controlled stage was also stored.

Sample chambers with an inner height of approximately 125 μm were constructed with two parallel strips of parafilm as spacers between a microscope slide (Menzel-Gläser, Braunschweig, Germany) and a coverslip (#1.5, 0.16–0.19 mm, Menzel-Gläser). To seal the coverslip to the slide, the construct was lightly compressed under a 90 °C heat block for 15–20 mins. Bead samples were prepared by diluting polystyrene beads with 2.17 μm diameter [0.5% weight/volume (w/v), Spherotech Inc., Libertyville, Illinois] and silica beads with 2.1 μm diameter (10% w/v, Bangs Laboratories Inc., Fishers, Indiana) 25,000 to 40,000 times in demineralized water.

B. Measurement Protocol

An experiment consisted of the determination of the position of the coverslip surface, recording of dis-

placement fluctuation data at different distances to the surface, and the subsequent determination of trap stiffness.

We started each series of measurements by determining the position of the center of the bead relative to the surface. In the setup with the water-immersion objective, we used the reflection of the laser light from the coverslip–water interface to determine the zero position. When the focal plane of the laser is imaged onto the camera (trap and image parfocal), the reflected small fraction of the laser beam will produce the smallest laser spot on the camera when the reflecting surface reaches the focus. Starting from this point, we varied the distance of the focus to the coverslip by moving the stage with a differential micrometer with a readout resolution of 100 nm. In practice, the bead will be trapped slightly beyond the focus of the beam. This offset error in the distance was determined and corrected in the data analysis procedure (see Section 3).

In the setup with the oil-immersion objective, we determined the position of the piezo stage at which the bead touched the surface (distance to surface equals the bead radius) by driving the z direction of the piezo-controlled stage externally with a 0.033 Hz triangular voltage. When the bead touched the surface, the total intensity on the quadrant diode abruptly started to change.[26] The corresponding position of the piezo stage was determined in LabVIEW. Repeated measurements and averaging provided a measurement of surface position with a typical standard error of the mean (s.e.m.) of ± 25 nm. We changed the distance of the bead to the surface by moving the sample with the piezo stage that was controlled in LabVIEW. Since the position of the focus will change because of refraction and spherical aberrations, the actual distance of trapping position to surface, h_{bead}, will be somewhat smaller than the amount moved by the stage, h_{piezo}, when the focus is moved away from the surface by the oil-immersion objective. The refraction effect can be approximated by a small-angle correction[15]:

$$h_{\mathrm{bead}} = \frac{n_w}{n_g} h_{\mathrm{piezo}}, \tag{1}$$

where n_g and n_w are the refractive indices of water and glass, respectively. A more accurate approximation is in principle possible,[27,28] but the difference between the results is below our experimental error margin. Additionally, we ignored the fact that not only the position of the focus but also the position of the potential minimum for trapping is changed by spherical aberrations because the balance between scattering and gradient forces changes.[27]

After determining the position of the surface, we increased the distance between the bead and the surface stepwise, starting from the surface, collecting bead-position fluctuation data every 0.5 μm at distances smaller than 10 μm, every 1.0 μm at distances between 10 and 20 μm, every 2.0 μm at distances between 20 and 40 μm, and (only for the water-immersion objective) every 5.0 μm at distances to the surface larger than 40 μm. Note that these steps in distance refer to the physical movement of the stage or the objective. The actual distances were calculated as described in Eq. (1) when the oil-immersion objective was used. At a given distance to the surface, the Brownian motion of the bead was recorded for at least 15 s at a sampling rate of 20 kHz.

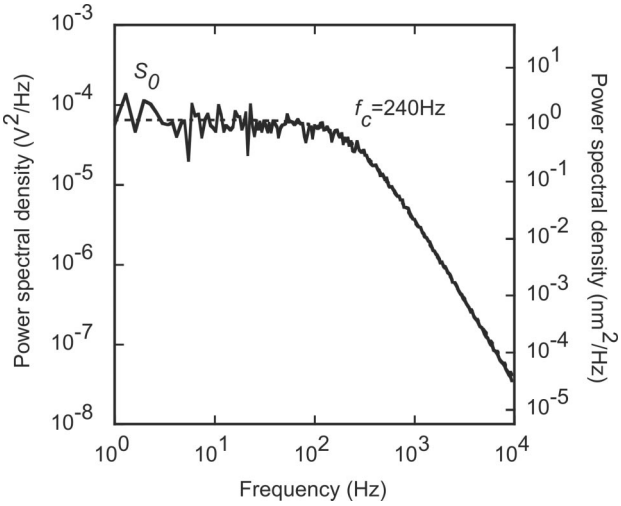

Fig. 2. Measured power spectral density (solid curve) of the thermal position fluctuations of a 2.1 μm silica bead in water, measured with a sample rate of 20 kHz for 15 s and smoothed by logarithmic binning. A Lorentzian (dashed curve) is fitted to the data. The left-hand axis is labeled in units of volts squared per hertz, the right-hand axis in nanometers squared per hertz with a detector response factor R of 7.45×10^{-8} m/V.

Because trap stiffness is linearly dependent on the light intensity, small changes in light intensity between different measurement series were corrected in the data analysis process by use of the measured total light intensity on the quadrant diode to scale the data sets to an average intensity.

C. Data Evaluation

A LabVIEW program was used to fit the power spectral density $S(f)$ of the displacement time series data to a Lorentzian, $S(f) = S_0 f_c^{\,2}/(f_c^{\,2} + f^2)$ (see Fig. 2). The corner frequency f_c of this Lorentzian determines the trap stiffness κ[24,29,30]:

$$\kappa = 2\pi\gamma f_c, \tag{2}$$

where γ is the drag coefficient for a bead with radius a in a fluid with viscosity η. At large distances from the surface, the drag coefficient is given by Stokes's law: $\gamma = 6\pi\eta a$. Close to the surface, the viscous drag coefficient increases according to Faxen's law[31,32]:

$$\gamma \approx \frac{6\pi\eta a}{\left[1 - \frac{9}{16}\left(\frac{a}{h}\right) + \frac{1}{8}\left(\frac{a}{h}\right)^3 - \frac{45}{256}\left(\frac{a}{h}\right)^4 - \frac{1}{16}\left(\frac{a}{h}\right)^5\right]}, \tag{3}$$

where h is the distance of the center of the bead to the coverslip surface. This approximation is valid in the proximity of one wall, in this case the coverslip surface, as long as $a \ll h$. During our experiments the beads were always more than 70 μm away from the second surface, the microscope slide. Its contribution could therefore be neglected. Note that this method to determine the trap stiffness does not require a calibration of the photodiode signal measured in volts to actual displacement in nanometers, but it is dependent on having an accurate value for the viscous drag that changes strongly in the vicinity of the surface. The result is therefore dependent on an accurate distance measurement.

To check both the applicability of Faxen's law and the accuracy of the distance measurement, we used a second method to determine trap stiffness in the case of the water-immersion objective. This (variance) method consisted of calculating the total mean-square displacement of the bead in the trap that, by equipartition, directly yields trap stiffness without the need to know the local viscous drag coefficient[29]:

$$\langle x^2(m^2)\rangle = \frac{k_B T}{\kappa}. \tag{4}$$

In this case knowledge of the calibration factor R of the detector, relating photodiode voltage to actual distance moved, is required. R also relates the power spectral density $S(f)$ in nanometers squared per hertz to $S^V(f)$ the power spectral density in volts squared per hertz by means of $S^V(f) = S(f)/R^2$. We calculate R from the high-frequency part of the power spectral density by using

$$\lim_{f \gg f_c} f^2 S^V(f) = f_c^{\,2} S_0^{\,V},$$

provided γ is known, as[30]

$$R(m/V) = \sqrt{\frac{k_B T}{\pi^2 \gamma f_c^{\,2} S_0^{\,V}}}. \tag{5}$$

We determined and averaged R from several measurements with bead–surface distances larger than 20 bead radii. At these large distances γ is essentially independent of the distance to the coverslip. We assume R does not change with distance to the surface when the water-immersion objective is used because there are no spherical aberrations present. In that case internally consistent results are the *a posteriori* justification of this assumption.

3. Results

Figure 3 shows how the corner frequency f_c of the lateral Brownian motion of a trapped bead increases when we are trapping deeper in the sample chamber (open symbols). Here we used the water-immersion objective. Since spherical aberration should not occur

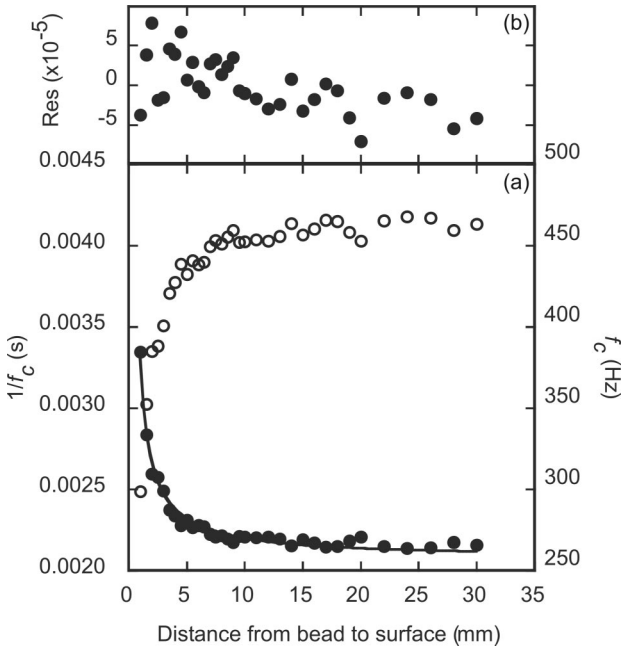

Fig. 3. (a) Dependence of the corner frequency of the Lorentzian fit to the power spectral density on the distance between bead and glass surface. A data set is shown for a silica bead, 2.1 μm in diameter, trapped with the water-immersion objective. Open circles are the corner frequency f_c (right-hand axis), closed circles $1/f_c$ (left-hand axis). We fitted Faxen's law [relation (3)] to $1/f_c$ with two free fitting parameters: the large-distance limit and an offset of the distance axis. (b) Residuals of the fit.

in this case, we expect the variation in f_c to stem entirely from the dependence of the drag coefficient on the distance to the surface [Faxen's law, relation (3)]. Consistent with this expectation, the change occurs within a few bead diameters from the surface, and f_c remains approximately constant at larger distances ($>10a$). To quantitatively verify this hypothesis, we fitted Faxen's law to the inverse of f_c (Fig. 3) with two fitting parameters, the large-distance limit and a distance correction Δh to compensate for the trap–focus offset and a possible error in the surface-position measurement. The sum of these two corrections can be accurately determined by the fit because of the rapid change of the drag coefficient near the surface. The total correction of distance Δh was approximately 0.28 ± 0.20 μm (s.e.m.). We found good agreement between the experimental data and Faxen's law (Fig. 3, residuals plot). Figure 4 shows the quality of the fit in a different way, by plotting the average of multiple data sets of lateral trap stiffness for both silica (circles) and polystyrene beads (squares), derived from measured f_c values by means of Eq. (2) (closed symbols). We used the corrected distance $h + \Delta h$ to calculate the drag coefficient needed in Eq. (2). For comparison, Fig. 4 also shows trap stiffness as found with the variance method (open symbols), which is not affected by the variation of the drag coefficient near the surface. We found agreement within measurement errors between the two results. The spread in trap stiffness over the

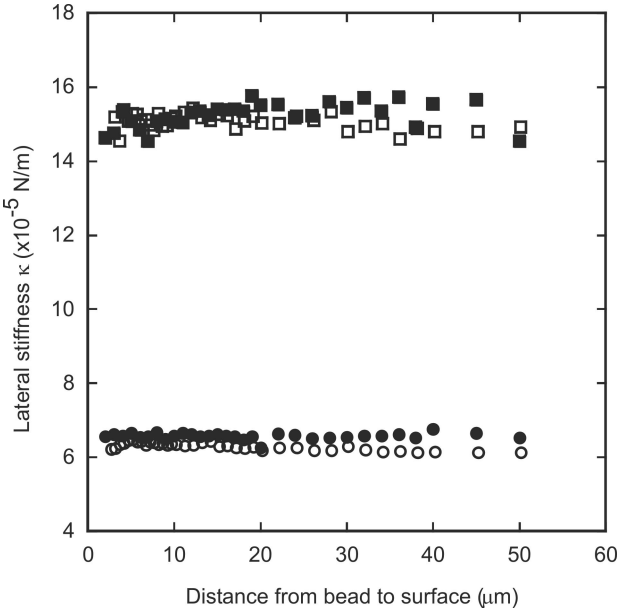

Fig. 4. Lateral trap stiffness as a function of the distance to the glass surface for silica beads (2.1 μm diameter, circles) and polystyrene beads (2.17 μm diameter, squares), trapped by the water-immersion objective. Closed symbols represent the results of the corner-frequency analysis; open symbols represent the results of the variance analysis. Each point in the graph is the average of at least two separate measurements.

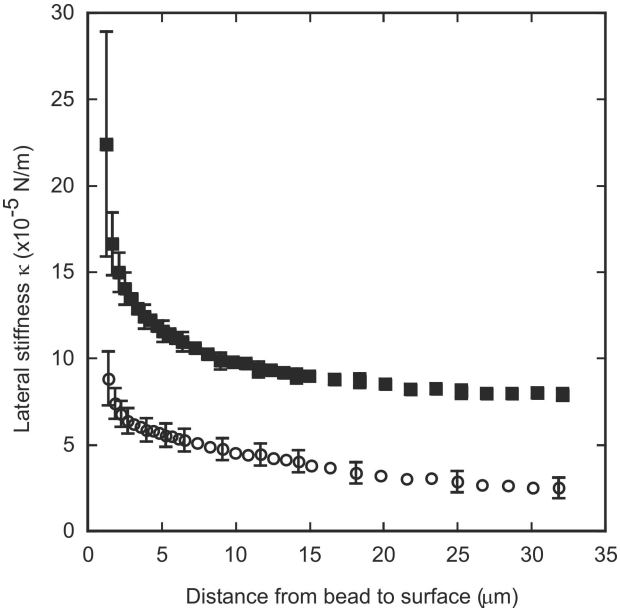

Fig. 5. Lateral optical-trap stiffness as a function of the distance to the glass surface for silica beads (2.1 μm diameter, circles) and polystyrene beads (2.17 μm diameter, squares), trapped with the oil-immersion objective. Trap stiffness was determined with the corner-frequency method. Data points in the graph are averages over multiple data sets. Error bars are calculated from uncertainties in bead radius and distance. Error bars are larger close to the surface because of the strong dependence of Faxen's law on bead radius and distance in this region. The distance of the bead to the surface is smaller than the distance traveled by the piezo stage because of refraction. We approximately corrected for this effect by using Eq. (1).

complete distance range was 5%–7%, whereas the estimated error per data point is of the order of a few percent. Comparing beads of different materials, but the same sizes, we found that the trap stiffness of polystyrene is more than twice that of silica (Fig. 4). A higher trap stiffness for polystyrene was expected from the index of refraction difference between the two materials.

In summary, these results confirm in an internally consistent manner that (1) Faxen's law is applicable for the increase of viscous drag near the surface, (2) for the water-immersion objective the calibration factor R for the detector measured at a large distance is valid for all distances, and (3) trap stiffness κ is independent of the focusing depth for the water-immersion objective.

Figure 5 shows the measured depth dependence of the lateral trap stiffness with the oil-immersion objective, i.e., in the presence of spherical aberrations, for both silica and polystyrene beads. We used Faxen's law directly to calculate γ, using the distance to the surface measured and refraction corrected as described in Section 2. As seen with the water-immersion objective, the trap stiffness for polystyrene beads was more than twice that for silica beads of approximately the same size. Figure 5 clearly shows a continuing decrease of the optical-trap stiffness with increasing distance to the surface. At small distances the error margins on the data increase because of the strong dependence of the viscous drag correction on bead radius and distance [relation (3)].

Axial trap stiffness is predicted to change even more drastically than lateral trap stiffness.[14] We used the corner-frequency method to qualitatively determine the dependence of the axial trap stiffness on the distance to the coverslip surface (Fig. 6). The data, which are noisier because the setup was mainly designed and optimized to measure lateral trap stiffness, was normalized to 1 at a distance of 10 μm to the surface for both data sets. The axial trap stiffness decreases with increasing distance to the surface, and this decrease follows approximately the same trend for both bead materials. For the water-immersion objective we did not observe a depth dependence for the axial trap stiffness, as expected (data not shown). The ratio was $\kappa_{z,\,\mathrm{silica}}/\kappa_{z,\,\mathrm{polystyrene}} = 0.45 \pm 0.02$, comparable with the ratios for these two materials in the lateral direction as determined with both the water- and oil-immersion objectives.

4. Discussion

The results in Figs. 3 and 4 of the measurements with the water-immersion objective are in agreement with theoretical expectation (see Fig. 1) and the experimental results of Capitanio *et al.*[13] For the oil-immersion objective, high-angle rays will increasingly lag behind the main focus when focusing deeper into the lower-index medium, with the limiting rays that are just at the critical angle for total internal reflection always remaining close to the interface (see Fig. 1). The focus

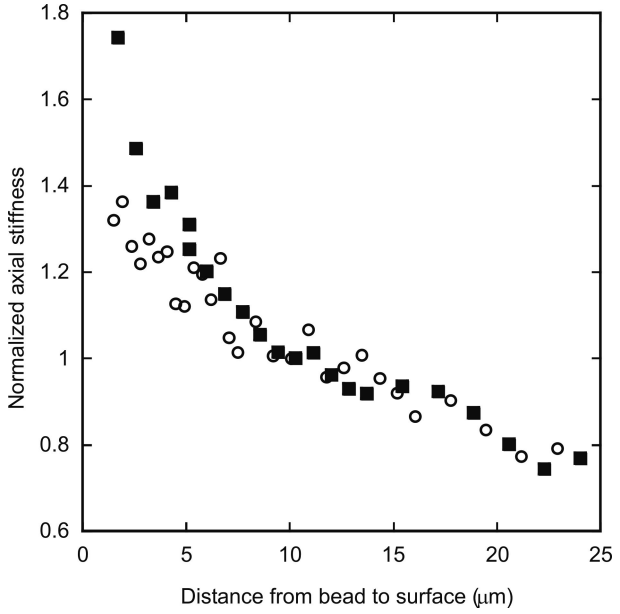

Fig. 6. Examples of the axial trap stiffness as a function of the distance between bead and glass surfaces for silica beads (2.1 μm diameter, circles) and polystyrene beads (2.17 μm diameter, squares), trapped with the oil-immersion objective. Trap stiffness was determined with the corner-frequency method. Data were taken under different conditions, and only the relative changes in trap stiffnesses are compared by normalization of the curves to 1 at a distance of 10 μm.

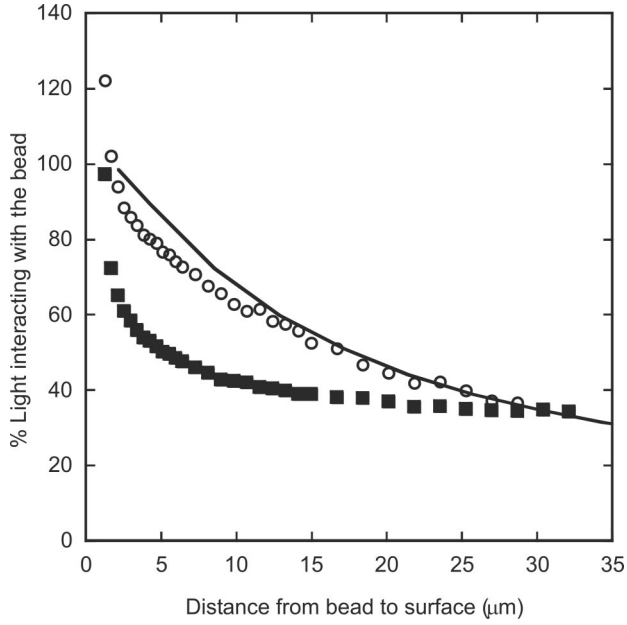

Fig. 7. Comparison of an approximate model with measured trap stiffnesses for silica beads (2.1 μm diameter, circles) and polystyrene beads (2.17 μm diameter, squares), trapped with the oil-immersion objective (see text). In this model, light intensity on the bead is a measure for trap stiffness. The experimental data are scaled to fit to the theoretical curve at large distances. Distance to the surface was calculated from stage displacement by use of Eq. (1).

will roughly maintain its lateral cross-sectional shape but will be smeared out in the axial direction with the maximum of intensity at the far end from the surface.[33] The trap will thus lose more and more high-angle rays that contribute strongly to the gradient force. We observed a monotonic decrease of trap stiffness for our 2 μm beads, consistent with expectation (see Fig. 5). We found in this study that the lateral trap stiffness rapidly decayed close to the surface and showed a more gradual decrease farther away. The experimental results of both Ghislain *et al.*[17] and Felgner *et al.*[20] for the lateral trap stiffness and trapping efficiency Q, respectively, for 1 μm polystyrene beads as functions of the distance also indicated a qualitatively similar behavior. The lateral trap stiffness for beads larger than the laser wavelength in the presence of spherical aberrations has not been calculated.

A. Modeling of Lateral Trap Stiffness

As a simple approximation we use the fact that the shape of the focus is hardly changing in the lateral direction and estimate the lateral trap stiffness as proportional to the light intensity near the maximum of the smeared focus, axially integrated over a bead radius. Wiersma *et al.*[33] provide a detailed analysis of the interference patterns that occur in the axial direction when the focus is distorted because of spherical aberrations occurring at a plane interface with index mismatch. They also present a simple stationary-phase approximation for the axial distribution of the focused light [their Eq. (20)]. We used this approximation to estimate the fraction of the total light intensity that interacts with a bead in the focus of the trap at different distances from the interface (see Fig. 7). The stationary-phase approximation is valid between the so-called paraxial and marginal shadow boundaries, where rays from the central and outermost parts of the objective pupil are focused, respectively, according to ray optics. The paraxial shadow boundary is equal to the location of the focus after refraction is taken into account [Eq. (1)]. We integrated the axial intensity distribution over a bead radius from the paraxial shadow boundary toward the surface and divided the result by the integral of the total axial intensity distribution between both shadow boundaries. Figure 7 shows relatively good correspondence between the thus-estimated trap stiffness and our data for silica beads, which were scaled to match the theoretical curve at the largest measured distances. The theoretical curve, because of the normalization by the total intensity, extrapolates to 100% at the surface. The measured trap stiffness, normalized to theory at large distances, reaches larger values close to the interface for silica beads. This is likely due to the lack of accuracy of our approximation. Furthermore, the theoretical curve lies systematically above the data for intermediate distances. This is most likely explained by the fact that we assumed that all light contributes equally to the optical gradient force and thereby the trap stiffness. High-angle rays, in fact, contribute more than paraxial rays, and the former

are rapidly lost from the focal intensity maximum because of aberration when focusing deeper into the water.

For polystyrene beads the mismatch between the theoretical curve and the data is more pronounced (Fig. 7). This is not unexpected because our treatment implicitly assumes that the field distributions are not influenced by the presence of the bead (Raleigh–Debye approximation). Although this is a reasonable assumption for silica beads (index ratio $\sim 1.38/1.33 = 1.04$), it is less valid for polystyrene beads (index ratio $\sim 1.5/1.33 = 1.13$).

B. Axial Trap Stiffness

In the axial direction one might expect a larger decrease in the trap stiffness than in the lateral direction because the peak light intensity decreases and spherical aberrations alter the shape of the focus more in the axial than in the lateral direction. However, we observed an approximate threefold decrease in trap stiffness for polystyrene beads when focusing at 25 μm distance from the surface, comparable with the decrease observed in the lateral stiffness. Experimental data from Wright *et al.*[18] and Felgner *et al.*[20] show a similar depth dependence of the axial trapping efficiency Q, both in magnitude and in shape. In Felgner *et al.*[20] the silica beads were in the same size range (diameters of 2.70 and 1.20 μm) as that of the beads we use. For these beads the decrease in Q_{ax} was also threefold to fourfold when focusing at 25 μm distance from the surface. Wright *et al.*[18] uses smaller silica beads (diameter of 1 μm), but this study contains only a small number of data points, and the maximum distance between the bead and the glass surface was 12 μm. The study of Ghislain *et al.*[17] contains too few data points in the axial direction to determine a trend in the data. Fällman and Axner calculated the depth dependence of the axial trap stiffness theoretically for beads in the micrometer-sized range.[15] They predict a slightly larger decrease in trap stiffness over the distance range up to a distance of 10 bead radii than what we find, but qualitatively our data agree with their calculations.

5. Conclusions

We have quantitatively mapped out the effect of spherical aberration on an optical trap formed in a watery solution by an oil-immersion objective. Our data can be explained by a simple model based on the loss of intensity in the focus, albeit that the agreement is closer for silica than for polystyrene beads. A better model for the lateral stiffness of the trap for beads larger than the trapping wavelength is still needed. When a water-immersion objective was used, i.e., in the absence of spherical aberrations, the lateral trap stiffness was independent of the distance to the surface, as expected. We have shown that this independence can be used to precisely determine the distance of the bead to the surface.

When water- and oil-immersion objective data are compared, it is seen that the advantage of a water-immersion objective is that trap stiffness is maintained even at large distances from the surface. An oil-immersion objective, however, traps stronger very close to the surface and is necessary, for example, in some single-molecule fluorescence techniques.

We thank Taco Visser for stimulating discussions and Erwin Peterman and Joost van Mameren for technical help. This work was supported by the Stichting voor Fundamenteel Onderzoek der Materie, which is financially supported by the Nederlandse Organisatie voor Wetenschappelijk Onderzoek.

References

1. A. Ashkin, J. M. Dziedzic, J. E. Bjorkholm, and S. Chu, "Observation of a single-beam gradient force optical trap for dielectric particles," Opt. Lett. **11,** 288–290 (1986).
2. G. J. L. Wuite, S. B. Smith, M. Young Keller, and C. Bustamante, "Single-molecule studies of the effect of template tension on T7 DNA polymerase activity," Nature (London) **404,** 103–106 (2000).
3. M. D. Wang, M. J. Schnitzer, H. Yin, R. Landick, J. Gelles, and S. M. Block, "Force and velocity measured for single molecules of RNA polymerase," Science **282,** 902–907 (1998).
4. K. Svoboda, C. F. Schmidt, B. J. Schnapp, and S. M. Block, "Direct observation of kinesin stepping by optical trapping interferometry," Nature (London) **365,** 721–727 (1993).
5. J. T. Finer, R. M. Simmons, and J. A. Spudich, "Single myosin molecule mechanics—piconewton forces and nanometer steps," Nature (London) **368,** 113–119 (1994).
6. J. E. Molloy, J. E. Burns, J. Kendrickjones, R. T. Tregear, and D. C. S. White, "Movement and force produced by a single myosin head," Nature (London) **378,** 209–212 (1995).
7. M. J. deCastro, R. M. Fondecave, L. A. Clarke, C. F. Schmidt, and R. J. Stewart, "Working strokes by single molecules of the kinesin-related microtubule motor ncd," Nat. Cell Biol. **2,** 724–729 (2000).
8. A. D. Mehta, R. S. Rock, M. Rief, J. A. Spudich, M. S. Mooseker, and R. E. Cheney, "Myosin-V is a processive actin-based motor," Nature (London) **400,** 590–593 (1999).
9. R. S. Rock, S. E. Rice, A. L. Wells, T. J. Purcell, J. A. Spudich, and H. L. Sweeney, "Myosin VI is a processive motor with a large step size," Proc. Natl. Acad. Sci. USA **98,** 13655–13659 (2001).
10. D. E. Smith, S. J. Tans, S. B. Smith, S. Grimes, D. L. Anderson, and C. Bustamante, "The bacteriophage phi 29 portal motor can package DNA against a large internal force," Nature (London) **413,** 748–752 (2001).
11. R. J. Davenport, G. J. L. Wuite, R. Landick, and C. Bustamante, "Single-molecule study of transcriptional pausing and arrest by E-coli RNA polymerase," Science **287,** 2497–2500 (2000).
12. C. Veigel, M. L. Bartoo, D. C. S. White, J. C. Sparrow, and J. E. Molloy, "The stiffness of rabbit skeletal actomyosin cross-bridges determined with an optical tweezers transducer," Biophys. J. **75,** 1424–1438 (1998).
13. M. Capitanio, G. Romano, R. Ballerini, M. Giuntini, F. S. Pavone, D. Dunlap, and L. Finzi, "Calibration of optical tweezers with differential interference contrast signals," Rev. Sci. Instrum. **73,** 1687–1696 (2002).
14. A. Rohrbach and E. H. K. Stelzer, "Trapping forces, force constants, and potential depths for dielectric spheres in the presence of spherical aberrations," Appl. Opt. **41,** 2494–2507 (2002).
15. E. Fällman and O. Axner, "Influence of a glass-water interface on the on-axis trapping of micrometer-sized spherical objects by optical tweezers," Appl. Opt. **42,** 3915–3926 (2003).
16. E. L. Florin, A. Pralle, E. H. K. Stelzer, and J. K. H. Horber,

"Photonic force microscope calibration by thermal noise analysis," Appl. Phys. A **66,** S75–S78 (1998).
17. L. P. Ghislain, N. A. Switz, and W. W. Webb, "Measurement of small forces using an optical trap," Rev. Sci. Instrum. **65,** 2762–2768 (1994).
18. W. H. Wright, G. J. Sonek, and M. W. Berns, "Parametric study of the forces on microspheres held by optical tweezers," Appl. Opt. **33,** 1735–1748 (1994).
19. A. Buosciolo, G. Pesce, and A. Sasso, "New calibration method for position detector for simultaneous measurements of force constants and local viscosity in optical tweezers," Opt. Commun. **230,** 357–368 (2004).
20. H. Felgner, O. Müller, and M. Schliwa, "Calibration of light forces in optical tweezers," Appl. Opt. **34,** 977–982 (1995).
21. G. J. L. Wuite, R. J. Davenport, A. Rappaport, and C. Bustamante, "An integrated laser trap/flow control video microscope for the study of single biomolecules," Biophys. J. **79,** 1155–1167 (2000).
22. E. J. G. Peterman, F. Gittes, and C. F. Schmidt, "Laser-induced heating in optical traps," Biophys. J. **84,** 1308–1316 (2003).
23. M. W. Allersma, F. Gittes, M. J. deCastro, R. J. Stewart, and C. F. Schmidt, "Two-dimensional tracking of ncd motility by back focal plane interferometry," Biophys. J. **74,** 1074–1085 (1998).
24. F. Gittes and C. F. Schmidt, "Interference model for back-focal-plane displacement detection in optical tweezers," Opt. Lett. **23,** 7–9 (1998).
25. A. Pralle, M. Prummer, E. L. Florin, E. H. K. Stelzer, and J. K. H. Horber, "Three-dimensional high-resolution particle tracking for optical tweezers by forward scattered light," Microsc. Res. Tech. **44,** 378–386 (1999).
26. M. J. Lang, C. L. Asbury, J. W. Shaevitz, and S. M. Block, "An automated two-dimensional optical force clamp for single molecule studies," Biophys. J. **83,** 491–501 (2002).
27. K. C. Neuman, E. A. Abbondanzieri, and S. M. Block, "Measurement of the effective focal shift in an optical trap," Opt. Lett. **30,** 1318–1320 (2005).
28. S. H. Wiersma, P. Torok, T. D. Visser, and P. Varga, "Comparison of different theories for focusing through a plane interface," J. Opt. Soc. Am. A **14,** 1482–1490 (1997).
29. K. Svoboda and S. M. Block, "Biological applications of optical forces," Annu. Rev. Biophys. Biomol. Struct. **23,** 247–285 (1994).
30. F. Gittes and C. F. Schmidt, "Signals and noise in micromechanical measurements," in *Methods in Cell Biology,* M. Sheetz, ed. (Academic, 1998), Vol. 55, pp. 129–156.
31. H. Faxen, "Die bewegung einer Starren Kugel längs der Achse eines mit zäher Flüssigkeit gefüllten Rohres," Ark. Mat. Astron. Fys. **17,** 1–28 (1923).
32. J. Happel and H. Brenner, *Low Reynolds Number Hydrodynamics* (Noordhoff, 1973).
33. S. H. Wiersma, T. D. Visser, and P. Torok, "Annular focusing through a dielectric interface: scanning and confining the intensity," Pure Appl. Opt. **7,** 1237–1248 (1998).